

## A Carbon-enhanced Lyman Limit System: Signature of the First Generation of Stars?

SIWEI ZOU,<sup>1,2</sup> PATRICK PETITJEAN,<sup>2</sup> PASQUIER NOTERDAEME,<sup>2</sup> CÉDRIC LEDOUX,<sup>3</sup> RAGHUNATHAN SRINAND,<sup>4</sup>  
LINHUA JIANG,<sup>1</sup> AND JENS-KRISTIAN KROGAGER<sup>2</sup>

<sup>1</sup>*Kavli Institute for Astronomy and Astrophysics, Peking University, Beijing 100871, China; zousiwei@pku.edu.cn*

<sup>2</sup>*Sorbonne Université, CNRS, UMR 7095, Institut d'Astrophysique de Paris, 98 bis bd Arago, 75014 Paris, France*

<sup>3</sup>*European Southern Observatory, Alonso de Córdova 3107, Casilla 19001, Vitacura, Santiago, Chile*

<sup>4</sup>*Inter-University Center for Astronomy and Astrophysics, Post Bag 4, Ganeshkhind, 411 007 Pune, India*

(Received; Revised; Accepted)

### ABSTRACT

We present the study of a Lyman limit system (LLS) at  $z_{\text{abs}} = 1.5441$  towards quasar J134122.50+185213.9 observed with VLT X-shooter. This is a very peculiar system with strong C I absorption seen associated with a neutral hydrogen column density of  $\log N(\text{H I}) (\text{cm}^{-2}) = 18.10$ , too small to shield the gas from any external UV flux. The low ionization absorption lines exhibit a simple kinematic structure consistent with a single component. Using CLOUDY models to correct for ionization, we find that the ionization parameter of the gas is in the range  $-4.5 < \log U < -4.2$  and the gas density  $-1.5 < \log n(\text{H}) (\text{cm}^{-3}) < -1.2$ . The models suggest that carbon is overabundant relative to iron,  $[\text{C}/\text{Fe}] > +2.2$  at  $[\text{Fe}/\text{H}] \sim -1.6$ . Such a metal abundance pattern is reminiscent of carbon-enhanced metal-poor stars detected in the Galaxy halo. Metal enrichment by the first generation of supernovae provide a plausible explanation for the inferred abundance pattern in this system.

*Keywords:* Quasar absorption line spectroscopy (1317); Lyman limit systems (981); CEMP stars (2105)

### 1. INTRODUCTION

The metal content of metal-poor stars is an important clue to understanding how the first objects in the Universe were enriched and how star-formation proceeded at that time (see Frebel & Norris 2015 for a review and references therein). Since massive metal-free stars (Population III stars) formed from the primordial gas and then exploded as the first generation of supernovae, the gas enriched by these first supernovae will form the main source of next generation of long-lived low-mass stars, which can be detected in the halo of our Galaxy today. Thus, studies of either metal-poor stars and/or the interstellar medium (ISM) generating them are of critical importance for understanding the chemical enrichment history in the early Universe.

Carbon enhancement has been detected in a large fraction of metal-poor stars, especially those at  $[\text{Fe}/\text{H}] < -4.5$  (Beers et al. 1992b; Cayrel et al. 2004; Beers & Christlieb 2005; Norris et al. 2007; Suda et al. 2008; Carollo et al. 2010; Frebel 2010; An et al. 2013; Nordlander et al. 2019). These carbon-enhanced metal-poor (CEMP) stars have first been studied by Beers et al. (1992a) who defined these stars as having  $[\text{C}/\text{Fe}] >$

$+1.0$ . Consensus on explaining metallicities in CEMP stars has not been reached yet. Several possibilities have been put forward to explain the peculiar abundance patterns in these stars (Carollo et al. 2012). One option is that they result from mass transfer from a now-extinct asymptotic giant branch (AGB) companion star (Herwig 2005). In that case, the produced CEMP star exhibits enhancements in s-process neutron-capture elements during its thermally pulsating AGB phase and is thus labeled CEMP-*s* star. This binary system model is supported by observed radial velocity variations of these stars (Lucatello et al. 2005; Placco et al. 2013; Starkenburg et al. 2014). Models have been built to interpret the abundances of CEMP-*s* stars (Fujimoto et al. 2000; Iwamoto et al. 2004; Bisterzo et al. 2012). Half of CEMP-*s* stars also exhibit strong enhancement in r-process elements (e.g. Eu), this subset is labeled as CEMP-*r/s* stars. Interpretation of this branch of stars is highly debatable, one assumption is that it forms out of a molecular cloud enriched by supernova ejecta (Bisterzo et al. 2011). Alternatively, the carbon enhancement may be the result of the explosion of Population III stars (Tominaga et al. 2007; Nomoto et al. 2013), that

seeded (with high carbon abundance) the proto-stellar cloud of the star we see today. These are known as CEMP-no stars ( $[\text{Ba}/\text{Fe}] < 0$ ), as they show no strong enhancement in their neutron-capture elements. Perhaps the empirical evidence in support of this picture is the observation of an increasing carbon enhancement with decreasing metallicity (Beers & Christlieb 2005; Aoki et al. 2007). Several scenarios have been suggested for the origins of CEMP-no stars (Norris & Yong 2019), e.g. mixing and fallback in the minihalos (Umeda & Nomoto 2003; Iwamoto et al. 2005; Nomoto et al. 2013); spinstars (Meynet et al. 2006; Maeder et al. 2015); binarity (Suda et al. 2004) and metal inhomogeneous mixing (Hartwig & Yoshida 2019).

Detecting gas exhibiting similar abundance patterns as metal-poor stars would open a new window to investigate the imprint of the first objects in the early universe. Damped Lyman- $\alpha$  (DLA) systems, with  $\log N(\text{H I}) > 20.3$  (Wolfe et al. 2005), trace most of the neutral gas in the Universe. They are considered to be intimately related to the progenitors of galaxies at high redshift. A CEMP-DLA at  $z_{\text{abs}} = 2.340$  with  $[\text{Fe}/\text{H}] = -3$  and  $[\text{C}/\text{Fe}] = +1.53$  has been first detected by Cooke et al. (2011). However, the carbon enhancement may be less than originally thought due to thermal broadening effects (Dutta et al. 2014). Models of metal-free nucleosynthesis can successfully reproduce the observed abundance pattern for this DLA (Kobayashi et al. 2011b). Another DLA with  $[\text{C}/\text{Fe}] > +0.6$ ,  $[\text{Fe}/\text{H}] = -2.8$  at  $z = 3.07$  has been reported by Cooke et al. (2012). To date, partially ionized H I systems have not been detected yet with such high carbon enhancement over iron. Lyman limit systems (LLS), with  $17.2 < \log N(\text{H I}) < 20.3$ , trace optically thick gas with complex ionization and kinematic structure in the circumgalactic medium (see Tumlinson et al. 2017 and references therein). Prochaska et al. (2015) present the relative abundances of 157 high-dispersion (HD) LLSs at  $1.76 < z < 4.39$  and tentatively conclude that the LLSs exhibit super-solar  $\alpha/\text{Fe}$  ratios. In contrast, their  $[\text{Si}/\text{C}]$  ratio exhibits solar relative abundance. However, there are handful of metal-free LLS at  $z \sim 3$  (Fumagalli et al. 2011) and  $z = 4.391$  (Robert et al. 2019), which indicates the LLSs may also be a good place to look at for the imprints of Population III stars. Thus, highly carbon-enhanced and metal-poor LLSs at high redshift would be of particular interests for understanding peculiar nucleosynthetic processes in the early Universe. More detection of pristine gas clouds at high redshift helps to form any potential conclusion on metal-poor stars enrichment to their native ISM.

Recently, we have detected a LLS at  $z_{\text{abs}} = 1.5441$  with an enhanced carbon metallicity compared to iron,  $[\text{C}/\text{Fe}] \geq +2.2$  at  $[\text{Fe}/\text{H}] = -1.6$ . In this paper, we present the observations in Section 3 and the ionization corrections in Section 4. We discuss the possible origin of the gas in Section 5 and give a summary in Section 6.

## 2. OBSERVATION AND DATA PROCESSING

The present C I system, towards QSO J1341+1852, is part of the first sample of high redshift absorption systems selected based only on the presence of C I absorption. The sample contains 66 C I absorbers at  $z > 1.5$  (Ledoux et al. 2015). It has been obtained by systematically searching SDSS-DR7 (Abazajian et al. 2009) quasar spectra (Schneider et al. 2010) for C I absorption. It is complete for  $W_r(\text{C I } \lambda 1560) > 0.40 \text{ \AA}$ . Follow-up observation has been performed with the ESO Ultraviolet and Visual Echelle Spectrograph (UVES) spectrograph for 27 systems and the ESO/X-shooter spectrograph for 17 systems. Molecular gas and its properties in the whole sample are analysed by Noterdaeme et al. (2018). Metallicity measurements and near-infrared (NIR) detections for X-shooter observations are presented by Zou et al. (2018).

Emission redshift for this QSO is 2.00, RA and DEC are 13:41:22.51 and +18:52:14.0 respectively. The  $g$ -band magnitude of the QSO is 17.2. The instrument X-shooter (Vernet et al. 2011) covers the full wavelength range from 300 nm to  $2.5 \mu\text{m}$  at intermediate spectral resolution using three spectroscopic arms UV-blue(UVB), visible(VIS), and NIR. The two-dimensional (2D) and one-dimensional (1D) spectra were extracted using the X-shooter pipeline in its version 2.5.2 (Modigliani et al. 2010). Flux calibration has been performed using observations of standard stars provided by ESO. Generally, the final spectra are close to the nominal resolving power of  $R = 4350, 7450, \text{ and } 5300$  in the UVB, VIS and NIR arms, for slit widths of 1.0, 0.9, and 0.9 arcsec, respectively. The converted rest-frame velocity resolutions are 69, 40 and 57  $\text{km s}^{-1}$  respectively. Signal-to-noise (SNR) ratio per pixel achieved in the UVB, VIS and NIR arms for this object are 75, 80 and 22 respectively.

## 3. MEASUREMENTS

In this section, we present the observational results obtained from absorption lines seen in this system and derive the physical properties of the gas. In the following, all column densities  $N$  are in units of  $\text{cm}^{-2}$ . It must be noted that the system is very simple with only one metal component.

### 3.1. H I

The H I Lyman- $\alpha$  profile together with the associated C I and O I absorption are shown in Figure 1. The H I absorption is fitted with a Voigt profile using both the  $\chi^2$  - minimization softwares VPFIT (Carswell & Webb 2014) and VoigtFit (Krogager 2018). The main component with  $\log N(\text{H I}) = 18.04 \pm 0.05$  is at the same redshift as the C I and O I absorptions. There is an extra weaker component present at  $z = 1.5448$  with  $\log N(\text{H I}) = 15.60 \pm 0.19$  for  $b = 10 \text{ km s}^{-1}$ .

The SDSS spectrum of the quasar is presented in Figure 2 together with a QSO spectrum template from (Selsing et al. 2016). The dust attenuation of the quasar is small with  $A_V$  and  $E(B - V)$  of 0.09 and 0.033 respectively (Zou et al. 2018).

### 3.2. Metallicity derived from neutral oxygen

We define metallicity ( $Z$ ) of element X relative to solar as  $[X/H] = \log N(X/H) - \log N(X/H)_\odot$  and use solar abundances from Asplund et al. (2009). The oxygen metallicity, derived from  $N(\text{O I})$  and  $N(\text{H I})$ , is an accurate indicator of the overall metallicity. This is because O I and H I have similar ionization potentials and are coupled by resonant charge exchange reactions, then  $[\text{O}/\text{H}] = [\text{O I}/\text{H I}]$ . For  $\log N(\text{O I}) < 14$ , rest-frame equivalent width  $W_r$  and column density  $N$  follow a linear relation:

$$N(\text{cm}^{-2}) = 1.13 \times 10^{20} \frac{W_r(\text{\AA})}{\lambda^2(\text{\AA})f}, \quad (1)$$

where  $f$  is the oscillator strength. The measured rest-frame equivalent width of O I  $\lambda 1302$  is  $W_r = 0.08 \pm 0.01 \text{ \AA}$ . With  $f(\text{O I } \lambda 1302) = 0.048$ , we derive  $\log N(\text{O I}) = 14.05$  using the linear relation. The line is therefore probably saturated and this value is a lower limit. We therefore use two methods to constrain the column density and Doppler parameter: *a*) we fit the  $\lambda 1302$  line with Voigt profiles using  $b$  values of 5 to 10  $\text{km s}^{-1}$ ; *b*) we use the apparent optical depth (AOD) method converting velocity-resolved flux into column densities without prior information on the curve-of-growth or the component structure (Fox et al. 2005). The optical depth in each velocity pixel is given by  $\tau_v = \ln [F_c(v)/F(v)]$ , where  $F_c(v)$  is the continuum flux and  $F(v)$  is the absorbed flux. From the results of the two methods given in Table 1, we conclude that  $\log N(\text{O I})$  is in the range [14.36,15.10].

We estimate that a robust lower limit is  $\log N(\text{O I}) = 14.36$  (corresponding to  $b = 8.0 \text{ km s}^{-1}$ ) and the lower limit on the gas metallicity is  $\log Z_{\text{lim}} > [\text{O}/\text{H}]_{\text{lim}} = -0.37$  relative to solar. Note that this lower limit is consistent with the mean metallicity measured in other systems of the whole C I sample (Zou et al. 2018).

### 3.3. Neutral carbon

Since the ionization potential of neutral carbon (11.3 eV) is smaller than that of neutral hydrogen (13.6 eV), the detection of neutral carbon usually indicates the presence of neutral, cold, and well-shielded gas. However, at such a small  $N(\text{H I})$  as what we see here, the gas cannot be shielded from the external UV flux and is probably partially ionized and warm. It is therefore very surprising to observe C I in this system. This is a direct indication that the background UV flux incident on the cloud is very low and/or that the carbon metallicity is unusually high. Contrary to what would be expected from the first possibility, high-ionized ions C IV and Si IV are detected together with neutral and low-ionization species O I, C II, Fe II, Si II, Si III, Al II and Al III.

Thanks to the reasonable resolution and good signal-to-noise ratio of the spectrum, we can disentangle absorption from the C I ground state fine-structure levels. The fit is presented in Figure 1 with red, purple and yellow colors for the different levels respectively. We find that  $N(\text{C I}^*)/N(\text{C I})$  ranges between 0.03 and 0.63.

### 3.4. Iron

Multiple transition lines  $\lambda\lambda\lambda\lambda 1608, 2344, 2374, 2383$  of Fe II with very different oscillator strengths are detected. They are useful in determining the  $b$  value. The simultaneous fit of the five lines gives  $b = 6.0 \pm 2.5 \text{ km s}^{-1}$  and  $\log N(\text{Fe II}) = 12.96 \pm 0.04$ . The error in  $b$  is large and gives the range of possible  $b$  values. When  $b$  is varied from 5 to 10  $\text{km s}^{-1}$ ,  $\log N(\text{Fe II})$  is well constrained within a small range [12.86,12.94]. With  $b = 6 \text{ km s}^{-1}$  as indicated by the Fe II fit, the oxygen metallicity is  $\sim 0.6$  dex larger than the lower limit given above (see Table 1) and therefore about twice solar or larger.

### 3.5. Other metal lines

We assume the low and intermediate-ions arise from the same phase (i.e. same temperature, density and ionization parameter), so we apply the same  $b$  value range ( $b = 5, 6, 8, 10 \text{ km s}^{-1}$ ) as for Fe II onto all ions except C IV and Si IV. The fit results and profiles are presented in Table 1 and Figure 3. For Si, Si II  $\lambda 1304$  is blended with other lines, so we only fit Si II  $\lambda 1526$ . With  $b$  between 5–10  $\text{km s}^{-1}$ , we find that  $\log N(\text{Si II})$  is constrained within the range [13.62,13.87] and the ratio  $\log N(\text{Si III})/N(\text{Si II})$  is in the range [0.29,1.55]. This indicates that Si III is probably the main silicon ion and confirms that the gas is ionized. For  $b = 5 \text{ km s}^{-1}$ ,  $\log N(\text{C II}) = 17.94 \pm 0.05$ . In the following, we adopt  $16.40 \pm 0.24$  for  $b = 10 \text{ km s}^{-1}$  as a robust lower limit of  $\log N(\text{C II})$ . However, it should be realized that if we were

to adopt the  $b$  value derived from the fit of the Fe II lines, the carbon abundance could be an order of magnitude larger than what we will derive later.

In the fitting process, we find that  $b$  values smaller than  $10 \text{ km s}^{-1}$  are obviously too small to fit the high-ion C IV and Si IV absorptions, which indicates that C IV and Si IV may reside in a different phase of the same cloud. We therefore fitted absorption lines of these two ions with  $b$  values of  $30 \text{ km s}^{-1}$ . Si IV  $\lambda 1402$  is strongly contaminated by other lines so we only fit Si IV  $\lambda 1393$ .

### 3.6. Electron density

We can constrain the electron density using the observed population ratio of the two atomic sub-levels of the C II ground state. The lower panel in Figure 4 of Silva & Viegas (2002) gives the relation between the ratio  $n(\text{C II}^*)/n(\text{C II})$  and the electron density  $n_e$  under the assumption the gas is ionized and at  $T = 10,000 \text{ K}$ . Our observed  $\log N(\text{C II}^*)/N(\text{C II})$  is in the range  $[-4.05, -2.69]$ , so that we estimate the  $\log n_e$  is ranging from  $-2.5$  to  $-1.0$ . Note that we cannot use their calculation of the C I transitions because in our case the C I excitation is due to collisions with electrons and protons and not with neutral hydrogen (see their Figures 1 and 2). We will present the estimation of hydrogen density in Section 4.

## 4. IONIZATION CORRECTION

In this section, we will model the ionization state of the gas in the current system. Indeed, for systems with  $\log N(\text{H I}) < 19.3$ , ionization corrections can be important and metallicities cannot be derived directly using column densities of only neutral or singly-ionized species. This is contrary to what can be done in the case of DLAs. For this we use the photoionization code CLOUDY (Ferland et al. 2017) to model the ionization state of the gas. It is important to note that for low and intermediate ionization species, only one narrow absorption component is seen. Given this simple kinematic structure of this system, we assume that the system is a single cloud.

We firstly assume that the system is photo-ionized by the metagalactic ionizing UV background from Khaire & Srianand (2019) only. We add the cosmic microwave background (CMB) at  $z = 1.5441$ . Then we vary the hydrogen volume density  $\log n(\text{H}) \text{ (cm}^{-3}\text{)}$  within the range  $[-4, 0]$ , with the two stopping criteria,  $\log N(\text{H I}) = 18$  and  $T = 100 \text{ K}$ . Ionization state of the gas is described by the ionization parameter  $U = \frac{\Phi(H)}{n(H)c}$ , where  $\Phi(H)$  is the flux of ionizing photons. Therefore the ionization parameter  $\log U$  is in the range  $[-1.99, -5.99]$ . In

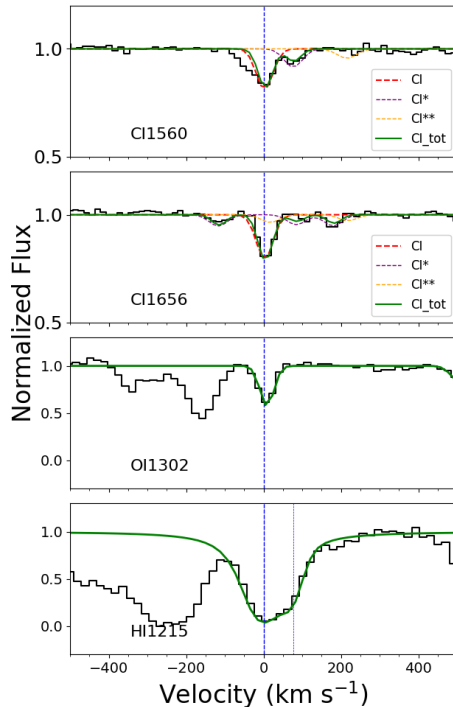


**Figure 1.** Voigt profile fits (green curve) to H I  $\lambda 1215$ , O I  $\lambda 1302$ , C I  $\lambda \lambda 1560, 1656$  absorption lines shown in velocity scale and centered at  $z = 1.5441$  in the J1341+1852 spectrum. Fits to the C I fine structure lines (C I\* and C I\*\*) are shown with purple and yellow dashed lines respectively. There is a second component of H I at  $z = 1.5448$  indicated by the vertical dotted line.)

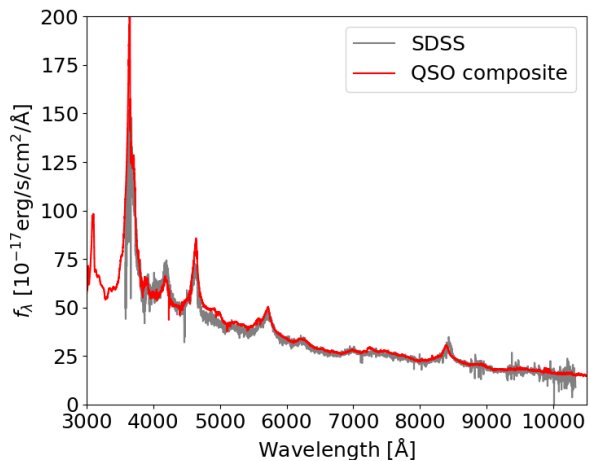


**Figure 2.** SDSS spectrum of J1341+1852 (in grey). The red curve is the X-shooter QSO composite template at  $1 < z < 2$  from Selsing et al. (2016). The template is not dust attenuated.

**Table 1.** Column densities ( $\log N$ ) derived for different assumed Doppler parameter values ( $b$ ) in the  $z = 1.5441$  absorption system toward J1341+1852. Both results from Voigt profile fits and AOD method are presented.

$z(\text{C I}) = 1.5441$					
Species	$\log N$ (VPFIT)				$\log N$ (AOD)
	$b=5.0 \text{ km s}^{-1}$	$b=6.0 \text{ km s}^{-1}$	$b=8.0 \text{ km s}^{-1}$	$b=10.0 \text{ km s}^{-1}$	
C I	$13.67 \pm 0.06$	$13.53 \pm 0.06$	$13.47 \pm 0.10$	$13.44 \pm 0.10$	$13.21 \pm 0.01$
C I*	$13.26 \pm 0.07$	$13.25 \pm 0.08$	$13.25 \pm 0.08$	$13.24 \pm 0.07$	
C I**	$< 12.54$	$< 12.25$	$< 12.51$	$< 12.71$	
C II	$17.90 \pm 0.05$	$17.58 \pm 0.18$	$17.56 \pm 0.19$	$16.40 \pm 0.24$	$> 14.35$
C II*	$13.85 \pm 0.12$	$13.74 \pm 0.10$	$13.72 \pm 0.09$	$13.71 \pm 0.07$	
Fe II	$12.94 \pm 0.04$	$12.96 \pm 0.04$	$12.86 \pm 0.05$	$12.82 \pm 0.05$	$12.76 \pm 0.01$
Mg II	$15.52 \pm 0.18$	$14.42 \pm 0.24$	$13.58 \pm 0.05$	$12.90 \pm 0.07$	$11.42 \pm 0.03$
Al II	$12.45 \pm 0.07$	$12.30 \pm 0.04$	$12.30 \pm 0.05$	$12.28 \pm 0.05$	$12.20 \pm 0.06$
Si II	$13.87 \pm 0.10$	$13.64 \pm 0.04$	$13.62 \pm 0.05$	$13.60 \pm 0.05$	$13.50 \pm 0.08$
Al III	$12.16 \pm 0.10$	$12.15 \pm 0.08$	$12.15 \pm 0.09$	$12.09 \pm 0.09$	$12.08 \pm 0.20$
Si III	$15.42 \pm 0.55$	$14.65 \pm 0.79$	$13.91 \pm 0.75$	$13.41 \pm 0.85$	$12.76 \pm 0.10$
O I	$15.10 \pm 0.39$	$14.60 \pm 0.16$	$14.36 \pm 0.23$	$14.40 \pm 0.10$	$14.39 \pm 0.01$
H I	$18.12 \pm 0.04$	$18.10 \pm 0.06$	$18.04 \pm 0.05$	$18.09 \pm 0.05$	$18.00 \pm 0.01$
H I <sup>a</sup>	$15.62 \pm 0.58$	$15.60 \pm 0.25$	$15.60 \pm 0.19$	$15.70 \pm 0.20$	
$b = 30.0 \text{ km s}^{-1}$					
C IV	$13.89 \pm 0.01$				
Si IV	$< 13.05$				

a. The second component of H I is at  $z = 1.5448$ .

**Table 2.** Parameters and outputs of photoionization models for the system at  $z_{\text{abs}} = 1.5441$  toward J1341+1852. The upper part of the Table shows the parameter ranges and steps used in the model. The lower part gives the results (column density, metallicities relative to solar and metallicity ratios) for the best-fit.

UV source	Parameters	min	max	Best Fit
KS19	$\log n(\text{H}) \text{ (cm}^{-3}\text{)}$	-4.00	0.00	$-1.5 \sim -1.2$
	$\log U$	-1.99	-5.99	$-4.5 \sim -4.2$
	$\log n_e \text{ (cm}^{-3}\text{)}$	-4.00	0.00	$-1.5 \sim -1.2$
	$T \text{ (K)}$	1,000	10,000	$9,000 \sim 9500$
Best-fit	[C I/C II]			-2.70
	[C II/C IV]			2.05
	[Fe II/Fe III]			-0.28
	[Si III/Si II]			-0.10
	[Si III/Si IV]			0.58
	[Fe/H]			-1.6
	[O/H]			0.0
	[C/H]			0.6
	[Si/H]			-1.3
	[Al/H]			-1.5
	[C/O]			0.6
	[C/Fe]			2.2
[Si/Fe]			0.4	
[Al/Fe]			0.1	

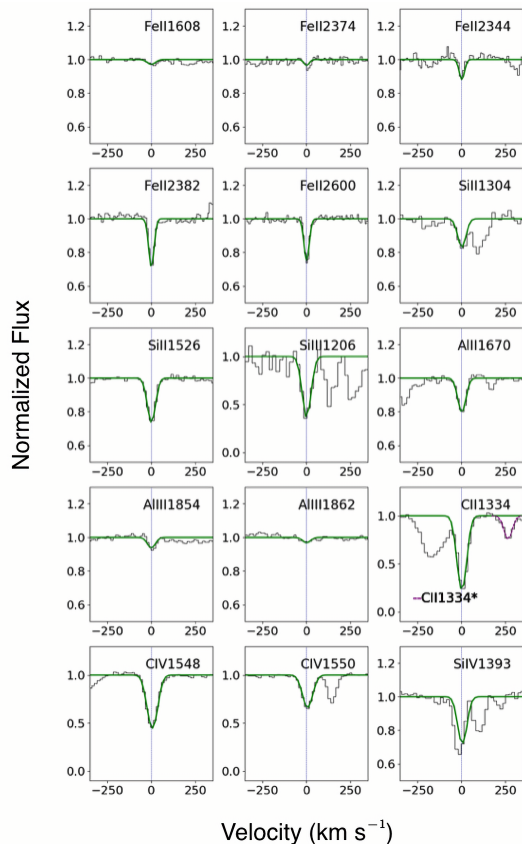


**Figure 3.** Voigt profile fits (green curve) of Fe II, Si II, Se, Al II, Al III and C II absorption lines. The Doppler parameter is  $b = 10 \text{ km s}^{-1}$ . For C IV and Si IV transition lines,  $b = 30 \text{ km s}^{-1}$ .

Figure 4, we plot the logarithmic column density ratios  $R$  of different ions as a function of  $\log U$ . Acceptable ranges derived from observations are indicated by colored points. We can tell that the ratios of low- and intermediate-ions can be reproduced within the range  $\log U = [-4.5, -4.2]$ . We also find that if relative solar metallicity is assumed, the column density ratios do not depend on the exact overall metallicity. With the metallicity varying between  $-2 < \log Z/Z_{\odot} < 1$ , the ratios  $\log N(\text{C III})/N(\text{C II})$  and  $\log N(\text{Si III})/N(\text{Si II})$  barely change. The ratio of  $\log N(\text{Si II})/N(\text{Fe II})$  is slightly higher at lower metallicity.

However, we find that with the same ionization parameter range (i.e. gas density range), the absolute column densities cannot be produced. At  $-4.5 < \log U < -4.2$ , we can reproduce  $N(\text{C I})$  and  $N(\text{O I})$  with  $\log Z/Z_{\odot} = 0.3$  and  $N(\text{C II})$  with at least  $\log Z/Z_{\odot} = 0.6$ . But the calculated  $\log N(\text{Fe II})$  at  $\log Z/Z_{\odot} = 0.6$  is in the range of  $[13.71, 14.90]$ , which is much larger than the observed upper limit  $\log N(\text{Fe II}) = 12.94$ . To reproduce the absolute observed Fe II column density, we have to

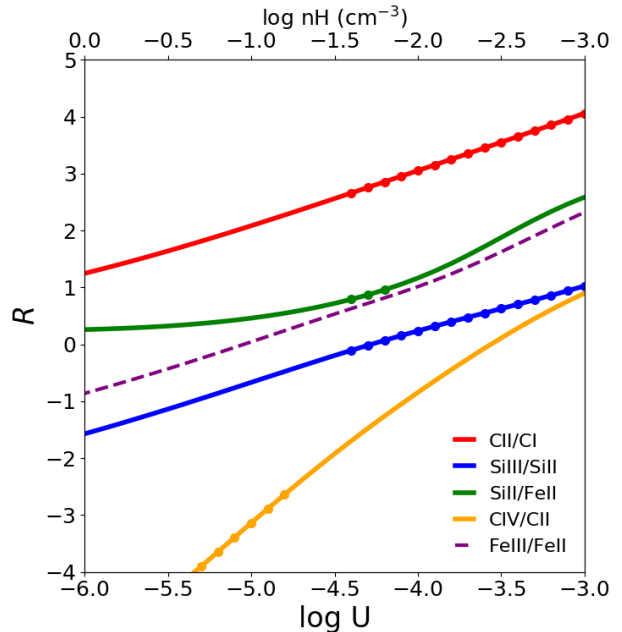


**Figure 4.** Column density ratios from CLOUDY models against ionization parameter  $\log U$ . Densities corresponding to  $U$  are given in the top axis. The ratios are plotted on a logarithmic scale. The ionizing flux is the metagalactic UV background from Khaire & Srianand (2019), abundance pattern is solar and overall metallicity is  $\log Z/Z_{\odot} = 0.3$ . Solid curves correspond to models, dots represent the observationally-allowed values.

decrease the iron metallicity to  $\log Z/Z_{\odot} \leq -1.4$ . This metallicity discrepancy between iron and carbon implies that the relative abundance of C over Fe should be at least 2.2 dex higher than the solar value. In addition, the relative C to O abundance should be larger than solar.

Therefore, as Figure 5 shows, we have to adjust the carbon abundance to 4 times higher than solar, Fe abundance to 0.02 times solar, Si abundance to 0.04 times solar and Al abundance to 0.03 solar. We then find that with  $-4.5 < \log U < -4.2$ , nearly all the column densities can be reproduced. The calculation parameter ranges and best-fit results are presented in Table 2. The optimal temperature range is between 9,000 – 9,500 K while we fix the density and metal abundances. We therefore conclude that  $[\text{C}/\text{Fe}] = +2.2$ ,  $[\text{C}/\text{O}] = +0.6$  at  $[\text{Fe}/\text{H}] = -1.6$ .

## 5. DISCUSSION

To summarize the CLOUDY models above, if we only consider the metagalactic background as the ionization

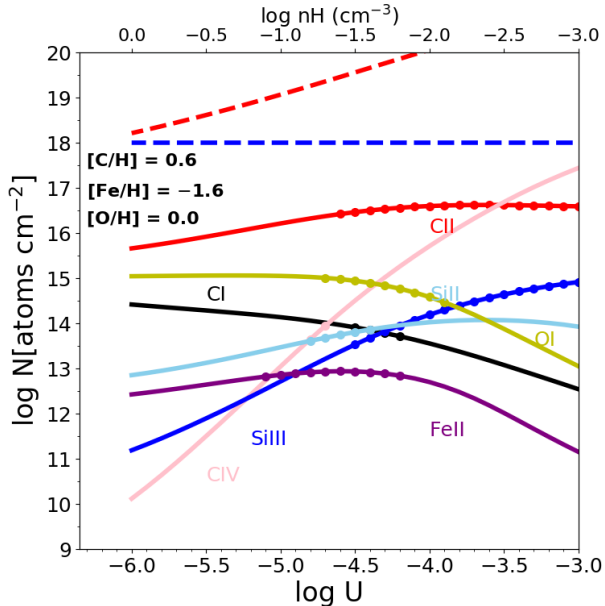


**Figure 5.** Ionization state modeling with UV metagalactic background from Khaire & Srianand (2019), abundance pattern is settled as non-solar with  $[C/H] = 0.6$  and  $[Fe/H] = -1.6$ . The best fit parameters and results are listed in Table 2. The solid curves are from models, dots are the range of values allowed by the observations.

source, we can reproduce the observed column densities with an ionization parameter in the range  $-4.5 < \log U < -4.2$ . The model also indicates that  $\log n_e = \log n(H)$  and should be close to  $-1.5$  which is consistent with our estimation in Section 3.6. Of course, the UV flux can be stronger due to the possible presence of nearby sources. In that case, the density would be larger. A factor of three larger would be acceptable. Column densities of C II, O I and Fe II cannot be reproduced with the same ionization parameter unless relative abundances are different from solar and large carbon enhancement is needed.

Given that the gas exhibits high carbon enhancement,  $[C/Fe] = +2.2$  at  $[Fe/H] = -1.6$ , we conjecture that the gas shares abundances similarity with CEMP stars. We discuss the possible scenarios that would yield such metal abundances and explain the origin of the gas in the following.

### 5.1. Depletion and extinction

Dust depletion is usually invoked to explain iron deficiency relative to carbon. We have shown however that the gas is highly ionized and warm. Although some depletion is likely, it cannot be as large as to explain what we observe. For this, the gas should be dense and cold as in our Galaxy. This is unlikely to be the case given

the low H I column density and the presence at the same time of highly ionized species. We should recall as well that we have used the lower limit for  $N(C II)$  and this column density is most probably larger. Furthermore, Fumagalli et al. (2016) constructed ionization models to investigate the properties of the HD-LLSs in Prochaska et al. (2015) and 77 LLSs from literature, they show that the LLSs at  $1.8 \leq z \leq 4.4$  are ionized and typically reside in environments with low dust content.

### 5.2. Scenario for the gas phase abundances

The most promising origin of the carbon enhancement is the production of metals in a core-collapse supernovae which undergoes mixing and fallback processes (Umeda & Nomoto 2003; Tominaga et al. 2007; Heger & Woosley 2010; Cooke & Madau 2014; Tominaga et al. 2014; Ishigaki et al. 2014). In this scenario, the explosion energy, progenitor mass, metallicity, and gravitational energy (Nomoto et al. 2013) are the key parameters affecting the final metal abundance pattern. When the explosion energy is not high enough to expel Fe-peak elements from the innermost layers, a large fraction of these elements eventually fall back onto the remnant. Therefore the interstellar gas polluted by the ejected gas will show some C and O enhancement with respect to Fe. This process leads to the generation of CEMP stars. Smaller explosion energy leads to larger fallback, thus with the same progenitor mass, higher  $[C/Fe]$ .

Umeda & Nomoto (2003) proposed that the core-collapse supernovae with a progenitor of mass  $20\text{--}130 M_{\odot}$  can explain the abundances observed in C-rich stars. The hyper metal-poor star (HMP) HE 0107-5240 has relative abundances similar to what we observed (Collet et al. 2006). Different progenitor masses, metallicity and explosion energy were adopted to explain the abundances of this HMP star. Most of them adopted  $M = 25 M_{\odot}$  as the progenitor mass and different explosion energy ( $E_{51} = E/10^{51}$  erg): 0.3 (Umeda & Nomoto 2003), 0.71 (Iwamoto et al. 2005), 1 (Ishigaki et al. 2014) and 5 (Tominaga et al. 2014). In addition, as shown in Figure 8 of Nomoto et al. (2013), the faint supernovae nucleosynthetic yields also match our carbon abundance relative to Fe ( $[C/Fe] = +2.2$ ). Similar metal relative abundances of our gas have also been detected in CEMP stars HE 2139-5432, HE 1150-0428, and G 77-61 (Tominaga et al. 2014).  $E_{51} = 5$  is set for the previous two stars and  $E_{51} = 1$  for the latter in the models in Tominaga et al. (2014). We therefore propose that our gas was enriched by core-collapse supernovae with  $> 20 M_{\odot}$  progenitor mass and a small explosion energy. The deficiency of Al and Si with respect to C and O that we

observe is also expected and further suggests that the gas has been enriched by faint supernovae.

It would be interesting to estimate the number of supernovae needed to enrich the gas we see to such metallicities. However, we have no information about the geometry of the cloud and especially the extension perpendicular to the line of sight. It seems probable however that several supernovae are needed. The region we observe is therefore probably peculiar in terms of environment.

We propose that the mixing and fallback scenario as the most promising origin of the carbon enhancement in the gas, however, other channels are not ruled out. The mixing and fallback scenario is applied to the explanation of CEMP-no stars, however, CEMP-no stars are mainly found at  $[\text{Fe}/\text{H}] < -2$ . Thus, to explain our  $[\text{Fe}/\text{H}]$ , an extra Fe contribution from a long-lived SN Ia is maybe a solution. Alternatively, low-mass ( $1\text{--}4 M_{\odot}$ ) AGB stars can provide carbon enhancement to the local ISM (Karakas 2010) 0.15 Gyr after the formation of the system (Kobayashi et al. 2011a). However, as shown in the yields by Kobayashi et al. (2011a), only low-mass AGB stars without faint supernovae cannot explain our  $[\text{C}/\text{Fe}]$  at  $z = 1.5441$ . Instead, our  $[\text{Fe}/\text{H}]$  may indicate the signature of CEMP- $r/s$  stars (e.g. BS 16080–175 with  $[\text{C}/\text{Fe}] = +1.8$  at  $[\text{Fe}/\text{H}] = -1.9$ , Allen et al. 2012). One possible scenario for this subset of CEMP stars is that they are formed in a binary system. The gas clouds, from which the binary system was born, was  $r$ -rich because of supernova explosions of previous-generation stars (Abate et al. 2016).

Nevertheless, with the present relative abundances of only a few elements along the line-of-sight, we cannot determine that the gas shares similar features with CEMP-no, CEMP- $s$ , or CEMP- $r/s$  stars, or fine-tune the actual enrichment history of this peculiar system. It would thus be of particular interest to obtain higher spectral resolution data to further investigate our conjecture and constrain better the physical state of this very peculiar gas.

## 6. SUMMARY

We have presented a detailed analysis of a very peculiar LLS at  $z_{\text{abs}} = 1.5441$  towards quasar J134122.50+185213.9.

1. Using X-Shooter data, we surprisingly detect C I absorption lines when the neutral hydrogen column density is small,  $\log N(\text{H I}) = 18.04 \pm 0.05$ . We derive a gas-phase overall metallicity lower limit of  $[\text{O}/\text{H}] = -0.37$ .

2. The kinematics of the system is simple with only one absorption component detected for neutral and singly ionized species.

3. We calculate the ionization correction with CLOUDY models. The gas is ionized with an ionization parameter of  $\log U = -4.5$  and a density  $\log n(\text{H}) \sim -1.5$  ( $\text{cm}^{-3}$ ). We show that oxygen is roughly solar,  $[\text{Fe}/\text{H}] \sim -1.6$ , and  $[\text{C}/\text{Fe}] = +2.2$ .

We suggest that the gas has been polluted by supernovae with  $M > 20 M_{\odot}$ , which have undergone a mixing fallback process.

4. It would be very difficult to avoid a carbon metallicity enhancement for this system. However, to derive the accurate metal abundances and the exact physical state of the gas and therefore settle the origin of this unusual set of metallicities, high-resolution spectroscopic data are crucially needed.

## ACKNOWLEDGEMENTS

We thank the anonymous referee for constructive comments and suggestions. SZ and LJ gratefully acknowledge support from the National Science Foundation of China (11721303, 11890693) and the National Key R&D Program of China (2016YFA0400703). PN, RS, and PPJ gratefully acknowledge support from the Indo-French Centre for the Promotion of Advanced Research (Centre Franco-Indien pour la Promotion de la Recherche Avancée) under contract No. 5504-B. PN and JKK acknowledge support from the French Agence Nationale de la Recherche under grant no ANR-17-CE31-0011-01 (project HIH2 PI Noterdaeme). We thank fruitful discussions with Sergei Balashev, Xiaoting Fu, Tilman Hartwig, Kohei Inayoshi and Chiaki Kobayashi, and valuable suggestions on the early version of manuscript by Zheng Cai and Ravi Joshi. We thank Sebastian Lopez and Thomas Krühler for help with the X-shooter data analysis.

## REFERENCES

- Abate, C., Stancliffe, R. J., & Liu, Z.-W. 2016, *A&A*, 587, A50, doi: [10.1051/0004-6361/201527864](https://doi.org/10.1051/0004-6361/201527864)
- Abazajian, K. N., Adelman-McCarthy, J. K., Agüeros, M. A., et al. 2009, *ApJS*, 182, 543, doi: [10.1088/0067-0049/182/2/543](https://doi.org/10.1088/0067-0049/182/2/543)

- Allen, D. M., Ryan, S. G., Rossi, S., Beers, T. C., & Tsangarides, S. A. 2012, *A&A*, 548, A34, doi: [10.1051/0004-6361/201015615](https://doi.org/10.1051/0004-6361/201015615)
- An, D., Beers, T. C., Johnson, J. A., et al. 2013, *ApJ*, 763, 65, doi: [10.1088/0004-637X/763/1/65](https://doi.org/10.1088/0004-637X/763/1/65)
- Aoki, W., Beers, T. C., Christlieb, N., et al. 2007, *ApJ*, 655, 492, doi: [10.1086/509817](https://doi.org/10.1086/509817)
- Asplund, M., Grevesse, N., Sauval, A. J., & Scott, P. 2009, *ARA&A*, 47, 481, doi: [10.1146/annurev.astro.46.060407.145222](https://doi.org/10.1146/annurev.astro.46.060407.145222)
- Beers, T. C., & Christlieb, N. 2005, *ARA&A*, 43, 531, doi: [10.1146/annurev.astro.42.053102.134057](https://doi.org/10.1146/annurev.astro.42.053102.134057)
- Beers, T. C., Preston, G. W., & Shectman, S. A. 1992a, *AJ*, 103, 1987, doi: [10.1086/116207](https://doi.org/10.1086/116207)
- Beers, T. C., Preston, G. W., Shectman, S. A., Doinidis, S. P., & Griffin, K. E. 1992b, *AJ*, 103, 267, doi: [10.1086/116060](https://doi.org/10.1086/116060)
- Bisterzo, S., Gallino, R., Straniero, O., Cristallo, S., & Käppeler, F. 2011, *MNRAS*, 418, 284, doi: [10.1111/j.1365-2966.2011.19484.x](https://doi.org/10.1111/j.1365-2966.2011.19484.x)
- . 2012, *MNRAS*, 422, 849, doi: [10.1111/j.1365-2966.2012.20670.x](https://doi.org/10.1111/j.1365-2966.2012.20670.x)
- Carollo, D., Beers, T. C., Chiba, M., et al. 2010, *ApJ*, 712, 692, doi: [10.1088/0004-637X/712/1/692](https://doi.org/10.1088/0004-637X/712/1/692)
- Carollo, D., Beers, T. C., Bovy, J., et al. 2012, *ApJ*, 744, 195, doi: [10.1088/0004-637X/744/2/195](https://doi.org/10.1088/0004-637X/744/2/195)
- Carswell, R. F., & Webb, J. K. 2014, VPFIT: Voigt profile fitting program, Astrophysics Source Code Library. <http://ascl.net/1408.015>
- Cayrel, R., Depagne, E., Spite, M., et al. 2004, *A&A*, 416, 1117, doi: [10.1051/0004-6361:20034074](https://doi.org/10.1051/0004-6361:20034074)
- Collet, R., Asplund, M., & Trampedach, R. 2006, *ApJL*, 644, L121, doi: [10.1086/505643](https://doi.org/10.1086/505643)
- Cooke, R., Pettini, M., & Murphy, M. T. 2012, *MNRAS*, 425, 347, doi: [10.1111/j.1365-2966.2012.21470.x](https://doi.org/10.1111/j.1365-2966.2012.21470.x)
- Cooke, R., Pettini, M., Steidel, C. C., Rudie, G. C., & Jorgenson, R. A. 2011, *MNRAS*, 412, 1047, doi: [10.1111/j.1365-2966.2010.17966.x](https://doi.org/10.1111/j.1365-2966.2010.17966.x)
- Cooke, R. J., & Madau, P. 2014, *ApJ*, 791, 116, doi: [10.1088/0004-637X/791/2/116](https://doi.org/10.1088/0004-637X/791/2/116)
- Dutta, R., Srianand, R., Rahmani, H., et al. 2014, *MNRAS*, 440, 307, doi: [10.1093/mnras/stu260](https://doi.org/10.1093/mnras/stu260)
- Ferland, G. J., Chatzikos, M., Guzmán, F., et al. 2017, *RMxAA*, 53, 385. <https://arxiv.org/abs/1705.10877>
- Fox, A. J., Savage, B. D., & Wakker, B. P. 2005, *AJ*, 130, 2418, doi: [10.1086/491735](https://doi.org/10.1086/491735)
- Frebel, A. 2010, *Astronomische Nachrichten*, 331, 474, doi: [10.1002/asna.201011362](https://doi.org/10.1002/asna.201011362)
- Frebel, A., & Norris, J. E. 2015, *ARA&A*, 53, 631, doi: [10.1146/annurev-astro-082214-122423](https://doi.org/10.1146/annurev-astro-082214-122423)
- Fujimoto, M. Y., Ikeda, Y., & Iben, Icko, J. 2000, *ApJL*, 529, L25, doi: [10.1086/312453](https://doi.org/10.1086/312453)
- Fumagalli, M., O'Meara, J. M., & Prochaska, J. X. 2011, *Science*, 334, 1245, doi: [10.1126/science.1213581](https://doi.org/10.1126/science.1213581)
- . 2016, *MNRAS*, 455, 4100, doi: [10.1093/mnras/stv2616](https://doi.org/10.1093/mnras/stv2616)
- Hartwig, T., & Yoshida, N. 2019, *ApJL*, 870, L3, doi: [10.3847/2041-8213/aaf866](https://doi.org/10.3847/2041-8213/aaf866)
- Heger, A., & Woosley, S. E. 2010, *ApJ*, 724, 341, doi: [10.1088/0004-637X/724/1/341](https://doi.org/10.1088/0004-637X/724/1/341)
- Herwig, F. 2005, *ARA&A*, 43, 435, doi: [10.1146/annurev.astro.43.072103.150600](https://doi.org/10.1146/annurev.astro.43.072103.150600)
- Ishigaki, M. N., Tominaga, N., Kobayashi, C., & Nomoto, K. 2014, *ApJL*, 792, L32, doi: [10.1088/2041-8205/792/2/L32](https://doi.org/10.1088/2041-8205/792/2/L32)
- Iwamoto, N., Kajino, T., Mathews, G. J., Fujimoto, M. Y., & Aoki, W. 2004, *ApJ*, 602, 377, doi: [10.1086/380989](https://doi.org/10.1086/380989)
- Iwamoto, N., Umeda, H., Tominaga, N., Nomoto, K., & Maeda, K. 2005, *Science*, 309, 451, doi: [10.1126/science.1112997](https://doi.org/10.1126/science.1112997)
- Karakas, A. I. 2010, *MNRAS*, 403, 1413, doi: [10.1111/j.1365-2966.2009.16198.x](https://doi.org/10.1111/j.1365-2966.2009.16198.x)
- Khaire, V., & Srianand, R. 2019, *MNRAS*, 484, 4174, doi: [10.1093/mnras/stz174](https://doi.org/10.1093/mnras/stz174)
- Kobayashi, C., Karakas, A. I., & Umeda, H. 2011a, *MNRAS*, 414, 3231, doi: [10.1111/j.1365-2966.2011.18621.x](https://doi.org/10.1111/j.1365-2966.2011.18621.x)
- Kobayashi, C., Tominaga, N., & Nomoto, K. 2011b, *ApJL*, 730, L14, doi: [10.1088/2041-8205/730/2/L14](https://doi.org/10.1088/2041-8205/730/2/L14)
- Krogager, J.-K. 2018, arXiv e-prints. <https://arxiv.org/abs/1803.01187>
- Ledoux, C., Noterdaeme, P., Petitjean, P., & Srianand, R. 2015, *A&A*, 580, A8, doi: [10.1051/0004-6361/201424122](https://doi.org/10.1051/0004-6361/201424122)
- Lucatello, S., Tsangarides, S., Beers, T. C., et al. 2005, *ApJ*, 625, 825, doi: [10.1086/428104](https://doi.org/10.1086/428104)
- Maeder, A., Meynet, G., & Chiappini, C. 2015, *A&A*, 576, A56, doi: [10.1051/0004-6361/201424153](https://doi.org/10.1051/0004-6361/201424153)
- Meynet, G., Ekström, S., & Maeder, A. 2006, *A&A*, 447, 623, doi: [10.1051/0004-6361:20053070](https://doi.org/10.1051/0004-6361:20053070)
- Modigliani, A., Goldoni, P., Royer, F., et al. 2010, in *Proc. SPIE*, Vol. 7737, Observatory Operations: Strategies, Processes, and Systems III, 773728, doi: [10.1117/12.857211](https://doi.org/10.1117/12.857211)
- Nomoto, K., Kobayashi, C., & Tominaga, N. 2013, *ARA&A*, 51, 457, doi: [10.1146/annurev-astro-082812-140956](https://doi.org/10.1146/annurev-astro-082812-140956)
- Nordlander, T., Bessell, M. S., Da Costa, G. S., et al. 2019, *MNRAS*, 488, L109, doi: [10.1093/mnrasl/slz109](https://doi.org/10.1093/mnrasl/slz109)
- Norris, J. E., Christlieb, N., Korn, A. J., et al. 2007, *ApJ*, 670, 774, doi: [10.1086/521919](https://doi.org/10.1086/521919)

- Norris, J. E., & Yong, D. 2019, *ApJ*, 879, 37,  
doi: [10.3847/1538-4357/ab1f84](https://doi.org/10.3847/1538-4357/ab1f84)
- Noterdaeme, P., Ledoux, C., Zou, S., et al. 2018, *A&A*, 612, A58, doi: [10.1051/0004-6361/201732266](https://doi.org/10.1051/0004-6361/201732266)
- Placco, V. M., Frebel, A., Beers, T. C., et al. 2013, *ApJ*, 770, 104, doi: [10.1088/0004-637X/770/2/104](https://doi.org/10.1088/0004-637X/770/2/104)
- Prochaska, J. X., O'Meara, J. M., Fumagalli, M., Bernstein, R. A., & Burles, S. M. 2015, *ApJS*, 221, 2,  
doi: [10.1088/0067-0049/221/1/2](https://doi.org/10.1088/0067-0049/221/1/2)
- Robert, P. F., Murphy, M. T., O'Meara, J. M., Crighton, N. H. M., & Fumagalli, M. 2019, *MNRAS*, 483, 2736,  
doi: [10.1093/mnras/sty3287](https://doi.org/10.1093/mnras/sty3287)
- Schneider, D. P., Richards, G. T., Hall, P. B., et al. 2010, *AJ*, 139, 2360, doi: [10.1088/0004-6256/139/6/2360](https://doi.org/10.1088/0004-6256/139/6/2360)
- Selsing, J., Fynbo, J. P. U., Christensen, L., & Krogager, J.-K. 2016, *A&A*, 585, A87,  
doi: [10.1051/0004-6361/201527096](https://doi.org/10.1051/0004-6361/201527096)
- Silva, A. I., & Viegas, S. M. 2002, *MNRAS*, 329, 135,  
doi: [10.1046/j.1365-8711.2002.04956.x](https://doi.org/10.1046/j.1365-8711.2002.04956.x)
- Starkeburg, E., Shetrone, M. D., McConnachie, A. W., & Venn, K. A. 2014, *MNRAS*, 441, 1217,  
doi: [10.1093/mnras/stu623](https://doi.org/10.1093/mnras/stu623)
- Suda, T., Aikawa, M., Machida, M. N., Fujimoto, M. Y., & Iben, Icko, J. 2004, *ApJ*, 611, 476, doi: [10.1086/422135](https://doi.org/10.1086/422135)
- Suda, T., Katsuta, Y., Yamada, S., et al. 2008, *PASJ*, 60, 1159, doi: [10.1093/pasj/60.5.1159](https://doi.org/10.1093/pasj/60.5.1159)
- Tominaga, N., Iwamoto, N., & Nomoto, K. 2014, *ApJ*, 785, 98, doi: [10.1088/0004-637X/785/2/98](https://doi.org/10.1088/0004-637X/785/2/98)
- Tominaga, N., Umeda, H., & Nomoto, K. 2007, *ApJ*, 660, 516, doi: [10.1086/513063](https://doi.org/10.1086/513063)
- Tumlinson, J., Peebles, M. S., & Werk, J. K. 2017, *ARA&A*, 55, 389,  
doi: [10.1146/annurev-astro-091916-055240](https://doi.org/10.1146/annurev-astro-091916-055240)
- Umeda, H., & Nomoto, K. 2003, *Nature*, 422, 871,  
doi: [10.1038/nature01571](https://doi.org/10.1038/nature01571)
- Vernet, J., Dekker, H., D'Odorico, S., et al. 2011, *A&A*, 536, A105, doi: [10.1051/0004-6361/201117752](https://doi.org/10.1051/0004-6361/201117752)
- Wolfe, A. M., Gawiser, E., & Prochaska, J. X. 2005, *ARA&A*, 43, 861,  
doi: [10.1146/annurev.astro.42.053102.133950](https://doi.org/10.1146/annurev.astro.42.053102.133950)
- Zou, S., Petitjean, P., Noterdaeme, P., et al. 2018, *A&A*, 616, A158, doi: [10.1051/0004-6361/201732033](https://doi.org/10.1051/0004-6361/201732033)